



Effect of Doping Manganese on the Morphological, Optical, and Thermal Properties of Zinc Oxide Nanoparticles Embedded on Poly-(p-anisidine)

K. Rathidevi^{*}, D. Tamilselvi² and N. Chithra³

¹Department of Chemistry, Kumaraguru College of Technology, Coimbatore, TN, India

²Department of Science and Humanities, Rathinam Technical Campus, Coimbatore, TN, India

³Department of Chemistry, Dr. Mahalingam College of Engineering and Technology, Pollachi, TN, India

Received: 07.07.2024 Accepted: 18.10.2024 Published: 30.12.2024

*rathichem@gmail.com



ABSTRACT

Metal-doped nanoparticles are of great interest for their multifunctionality and versatile applications. Recent research has focused on analyzing the morphological and optical properties of zinc oxide nanoparticles. Nanostructured materials find diverse uses as corrosion inhibitors, sunscreen agents, anti-scratch coatings, and stain removers, driving the need for novel materials with specific properties. The present work analyzed the structural, optical, and thermal properties of ZnO and Mn/ZnO nanoparticles, poly-(p-anisidine) (PPA), and ZnO-PPA, Mn/ZnO-PPA nanocomposites by various techniques including X-Ray diffraction, Fourier transform infra-red spectroscopy, scanning electron microscopy, energy dispersive studies, ultra-violet-visible spectroscopy, and photoluminescence studies. The XRD results confirmed the wurtzite type structure for all the synthesized nanoparticles, and no phase of impurity was noted. The SEM analysis confirmed the rod like structure with crystallites of hexagonal and spherical morphology for pure zinc oxide and nanoflower-like shape for all the manganese-doped nanoparticles and polymer nanocomposites. A very clear polymer cross-linkage chain formation for polymer nanocomposites was also observed. The ultraviolet-visible spectra results showed a red shift in absorption for ZnO-PPA, Mn/ZnO-PPA nanocomposites with reference to pure zinc oxide nanoparticles. The bandgap values are noted to be 3.20, 2.29, 2.89, 2.00 and 2.98 eV for pure ZnO, Mn/ZnO, PPA, ZnO-PPA and Mn/ZnO-PPA, respectively. The existence of elements such as Zn, O, Mn, C and N were evidenced by EDAX analysis. It also confirms the absence of impurities in the synthesized nanoparticles and PPA. Thermal studies showed a finite difference in the weight loss in the temperature range 25 °C to 900 °C. Three-different stages of thermal decomposition were observed in all the above synthesized nanomaterials.

Keywords: Zinc oxide; Nanoparticles; Poly-(p-anisidine); Manganese doping; Nanocomposites.

1. INTRODUCTION

Nanotechnology develops materials with novel physical and chemical properties and functions. There are noticeable nanostructured semiconducting materials having remarkable properties than their bulk materials. Zinc oxide nanoparticles are semiconducting materials having a wide band gap. They find a significant application in photocatalytic degradation, gas sensors, cosmetics, drug carriers, storage, displays for electrical and optical devices and solar cells. (Phongarthit *et al.* 2019; Bhargav *et al.* 2019). Various types of structures of zinc oxide such as nanoparticles, nanowires, nanorods and nanobelts have been synthesized by researchers in recent years (Safeen *et al.* 2022; Leprince-Wang *et al.* 2023). The properties of zinc oxide can be modified by doping with suitable elements. The multifunctional properties and versatile applications of mixed metal oxide nanoparticles have initiated a lot of interest among researchers to study their new properties and applications. Recently, much focus is given on doping of transition elements into zinc oxide lattice to enhance its

property (Djaja *et al.* 2020). Doping transition metals with zinc oxide paved the way to use zinc oxide in the field of spintronic devices. When transition metals are used as dopants, the size of the zinc oxide nanoparticles can be controlled, which helps improve their magnetic properties.

The properties of nanomaterials can also be improved by blending with polymeric chains (Begum *et al.* 2016; Singh *et al.* 2019). Polymer nanocomposites are promising materials which exhibit remarkable physical and chemical properties when compared to their parent constituents. These materials are also used as an alternative to conventional polymeric materials. The presence of conjugated π electrons in the long polymeric backbone makes some of the polymers conducting materials like metals. Polymer nanocomposites are widely used in energy storage, sensors, microelectronics, and magnetic electronics, etc. The present work explored the synthesis of pure ZnO and Mn/ZnO nanoparticles using the chemical precipitation method. Poly-(p-anisidine) and ZnO-PPA, Mn/ZnO-PPA nanocomposites were

synthesized by chemical oxidative polymerization method. The synthesized materials were characterized by XRD, FTIR, UV-Visible, PL, SEM, EDAX and TGA techniques.

2. EXPERIMENTAL SECTION

2.1 Synthesis of pure ZnO and Mn/ZnO Nanoparticles

Zinc nitrate hexahydrate (1 M) was dissolved in 100 mL of distilled water. To this, 100 mL of 2 M sodium hydroxide was added and continuously stirred for around 12 hours, whereupon the pH reached 12. The precipitate was filtered and washed with ethanol to remove contaminants. The moisture content was removed by dehydrating at 100°C in a hot-air oven. The dried precipitate was ground in an agate mortar, and the ground sample was annealed in a muffle furnace for two hours at 500°C. The pure zinc oxide nanoparticles were crushed, cooled, and kept in a container for further studies (K. Qi *et al.* 2020). The same procedure was used to synthesise Mn/ZnO nanoparticles by taking zinc nitrate hexahydrate (0.90 M) and manganese nitrate tetrahydrate (0.10 M). The synthesis is represented in Fig. 1.

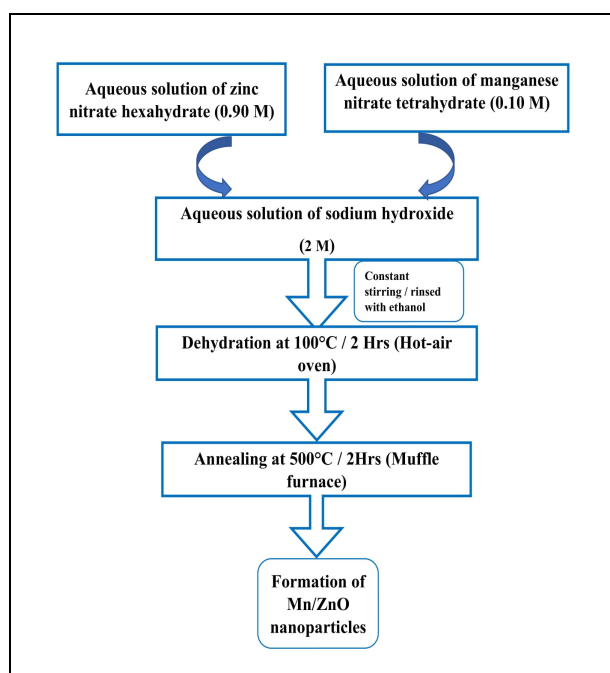


Fig. 1: Schematic diagram of synthesis of Mn/ZnO nanoparticles

2.2.1 Synthesis of Poly-(p-anisidine) (PPA), ZnO-PPA and Mn/ZnO-PPA

Poly-(p-anisidine) was prepared by chemical oxidation of the monomer p-anisidine in acidic conditions (HCl) using ammonium persulphate as the oxidising agent. About 12.31 g of p-anisidine monomer was added to 10 mL of 1.0 mol/L hydrochloric acid. The

mixture was then sonicated for approximately an hour to achieve uniform dispersion. Following thorough dispersion, the mixture was maintained in an ice bath (0-5 °C). Precooled ammonium persulphate (22.81 g) was added to the aforesaid solution dropwise while being continuously stirred. The polymerization reaction was continued by vigorous stirring for about 24 hours. Formation of a green precipitate indicates completion of the polymerization reaction. The ZnO-PPA / Mn/ZnO-PPA nanocomposite was synthesized following the above procedure by adding about 1.0 g of ZnO / Mn/ZnO nanoparticles into the monomer solution before adding ammonium per sulphate solution. The polymer / polymer nanocomposite was filtered and washed well with 1 M ammonium hydroxide under constant stirring for 3 hours. Then, the obtained product was rinsed with deionized water and finally washed with ethanol to eliminate the unreacted monomer and dehydrated at 100 °C for 6 hours. (Xiao *et al.* 2020).

3. RESULTS AND DISCUSSION

3.1 X-Ray Diffraction (XRD) Analysis

The structural characteristics, crystallite size, and phase purity of pure ZnO, Mn/ZnO nanoparticles, poly-(p-anisidine) (PPA) polymer, ZnO-PPA, and Mn/ZnO-PPA polymer nanocomposites were investigated by XRD analysis (Fig. 2). The peaks for Mn/ZnO can be found in this figure at $2\theta = 31.64, 34.30, 36.13, 47.42, 56.48, 62.74, 66.25, 67.83, \text{ and } 68.96$ degrees. These correspond to the (100), (002), (101), (102), (110), (103), (200), (112), and (201) planes, respectively. The absence of other impurity peaks suggests that the prepared samples are pure. The diffraction pattern for the Mn/ZnO nanoparticles confirmed that there are no structural changes. The diffraction peaks of this pattern suggest a hexagonal wurtzite structure, which is in perfect accordance with JCPDS card no.36-1451 (Bouzidi *et al.* 2018).

Absence of additional peaks in the case of Mn/ZnO evidently shows that the dopant has not changed the lattice structure of zinc oxide. This clearly reveals that zinc has been substituted by the dopant manganese in the zinc oxide lattice without altering the structure. Furthermore, the peak intensity for Mn/ZnO was found to decrease when compared to zinc oxide, which may be due to decreased grain size of doped nanoparticles. The broad peak at 26.5° indicates poly-(p-anisidine). The same peak was observed in the polymer nanocomposites. The polymer peak position has been shifted and the position of sharp (101) peak in the ZnO-PPA and Mn/ZnO-PPA. This clearly confirms the nanoparticles were embedded well on the polymer matrix (Ganesh *et al.* 2017).

The size of the synthesized nanoparticles was calculated as per Debye-Scherrer formula,

$$D = k\lambda/(\beta\cos\theta) \quad \dots (1)$$

In Eqn. 1, k is the shape factor ($=0.9$) Scherrer constant, λ is the X-ray wavelength (1.5418 \AA), β is the full width of half-maximum (FWHM) and θ is the Bragg diffraction angle.

The average crystallite size of the synthesised nanoparticles D was determined by applying the Debye-Scherrer formula was found to be 57.04, 53.66, 61.84, and 50.85 nm for pure ZnO, Mn/ZnO, ZnO-PPA and Mn/ZnO-PPA respectively. The addition of dopants into the zinc oxide lattice has reduced crystallite size of Mn/ZnO nanoparticles compared to ZnO nanoparticles.

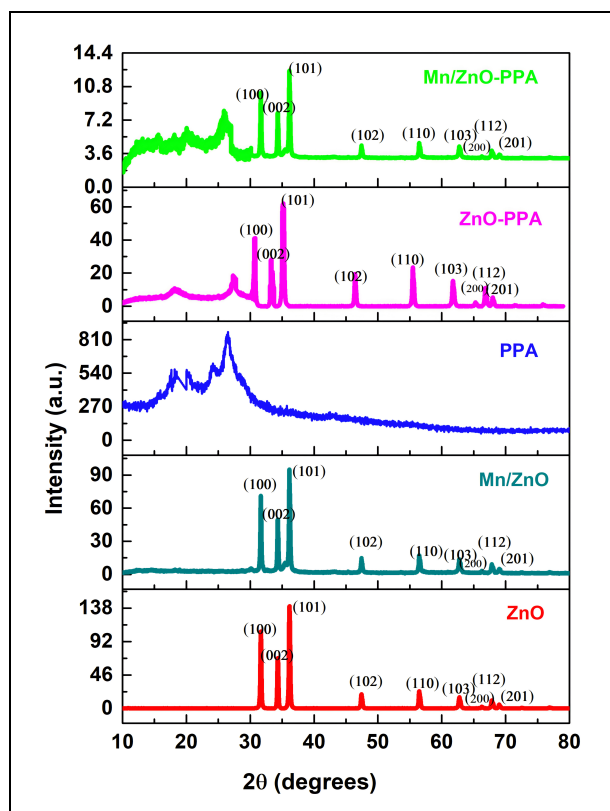


Fig. 2: XRD spectra of ZnO, Mn/ZnO, poly-(p-anisidine), ZnO-PPA and Mn/ZnO-PPA

3.2 Fourier Transform Infrared (FTIR) Spectroscopy Analysis

The FTIR spectra of ZnO, Mn-doped ZnO nanoparticles, poly-(p-anisidine), ZnO-PPA and Mn/ZnO-PPA polymer nanocomposites are shown in Fig. 3. The adsorption peak observed at 571 cm^{-1} for pure ZnO and 608 cm^{-1} for Mn/ZnO has been attributed due to the Zn-O stretching mode (Hoseinpour *et al.* 2018). The addition of manganese slightly altered the peak position of Zn-O stretching and causes additional peaks (Rajamanickam *et al.* 2014). The peak at 3508 cm^{-1} corresponds to the stretching vibrations of O-H of H_2O molecule. The peak at 1632 cm^{-1} is due to the

bending vibration of H-O-H of water molecules which confirms the presence of small amount of water in the zinc oxide nanoparticles. The peak at 1383 cm^{-1} is attributed to Mn-O stretching vibrations. zinc oxide lattice

The absorption peaks for the poly-(p-anisidine) (PPA) polymer at 3446 cm^{-1} corresponds to NH stretching mode and the peaks at 1564 cm^{-1} and 1511 cm^{-1} are due to the stretching vibrations of quinoid and benzenoid ring units, respectively. The peak at 1384 cm^{-1} is attributed to benzenoid ring C-N stretching mode. The characteristic absorption peak around 1251 cm^{-1} shows the presence of methoxy group in the aromatic ring. The noticeable peak at 1030 cm^{-1} attests the presence of C-O-C and the peak at 1111 cm^{-1} is due to C-N-C. The peak at 827 cm^{-1} confirms the aromatic C-H out of plane bending vibration mode. The absorption peaks of ZnO-PPA and Mn/ZnO-PPA are like that of PPA with very slight variation.

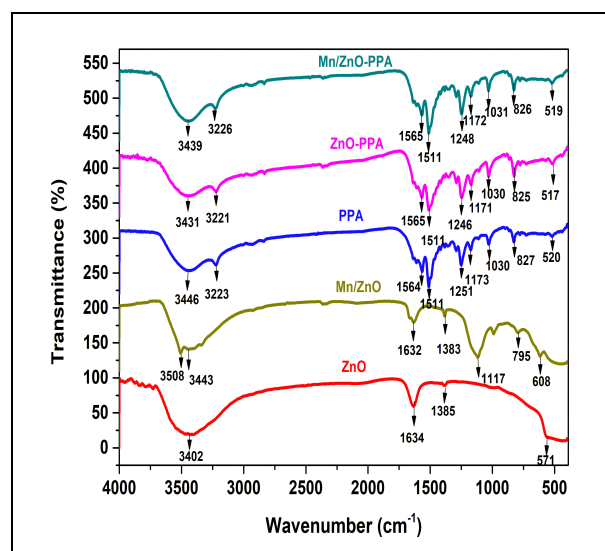


Fig. 3: FTIR spectra of ZnO, Mn/ZnO, PPA, ZnO-PPA and Mn/ZnO-PPA

3.3 Ultra-Violet Spectral Analysis

The UV spectra (Fig. 4) of pure ZnO, Mn/ZnO, PPA, ZnO-PPA and Mn/ZnO-PPA were recorded to study their optical properties. The peak at 351 nm for pure ZnO nanoparticles was red shifted to 363 nm on the addition of manganese as a dopant (Krishnaswamy *et al.* 2019). The electrons from valence bond were photoexcited to the conduction band resulting in a red shift. The absorption peak for PPA at 320 nm is due to the $\pi \rightarrow \pi^*$ transition of the benzenoid ring.

The peak at 328 nm and 354 nm for ZnO-PPA and Mn/ZnO-PPA polymer nanocomposites reveals the presence of $\pi - \pi^*$ transition of the benzenoid rings of the polymer. It was found that the addition of dopants into the polymer matrix shift the peak towards slightly longer wavelength than the pure polymer PPA. The addition of

dopant and polymer into zinc oxide structure results in red shift (Ahmad *et al.* 2014).

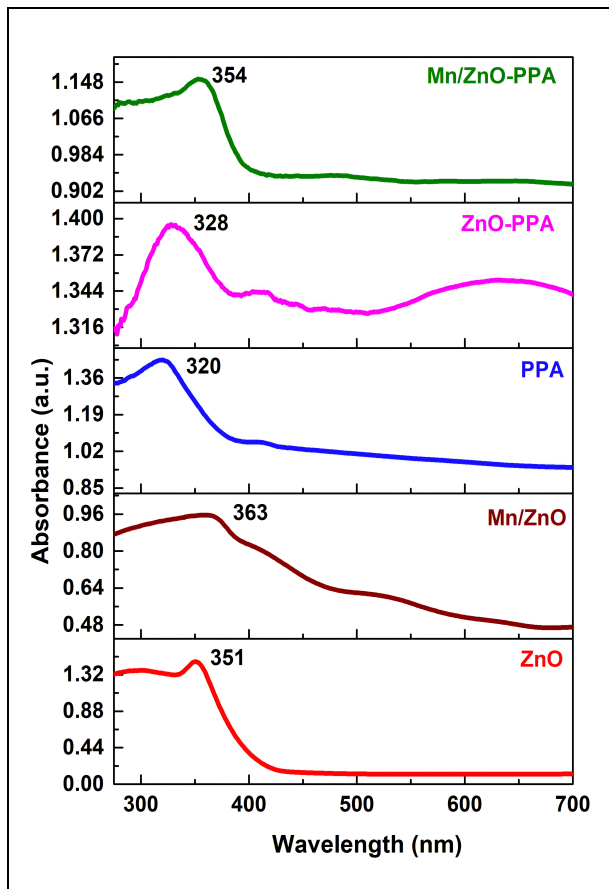


Fig. 4: UV-Vis spectra of ZnO, Mn/ZnO, PPA, ZnO-PPA and Mn/ZnO-PPA

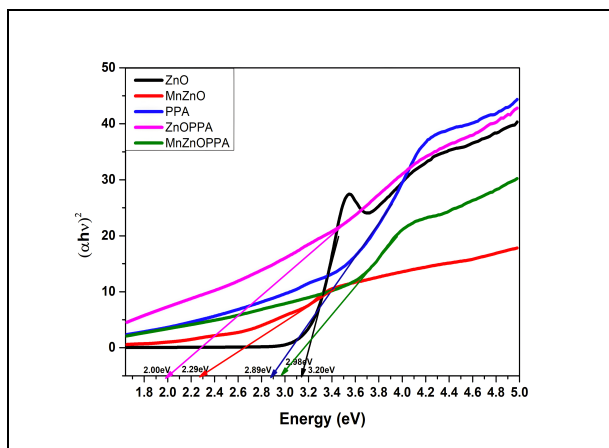


Fig. 5: Band-Gap spectra of ZnO, Mn/ZnO, ZnO-PPA and Mn/ZnO-PPA

The bandgap of pure ZnO nanoparticles was calculated by plotting a graph of $(\alpha h\nu)^2$ against binding energy using the below-mentioned formula,

$$(\alpha h\nu)n = A (h\nu - E_g) \quad \dots (2)$$

In Eqn. 2, $h\nu$ indicates photon energy, A indicates proportionality constant, α indicates absorption co-efficient, E_g indicates band gap energy, n values are $1/2$, $3/2$, 2 or 3 depending on the nature of absorption.

3.4 Bandgap Calculation

From Fig. 5, the bandgap values can be noted as 3.20, 2.29, 2.89, 2.00 and 2.98 eV for pure ZnO, Mn/ZnO, poly-(p-anisidine) (PPA), ZnO-PPA and Mn/ZnO-PPA polymer nanocomposites, respectively. From these values, it is evident that addition of dopants decreases the band gap of pure zinc oxide nanoparticles.

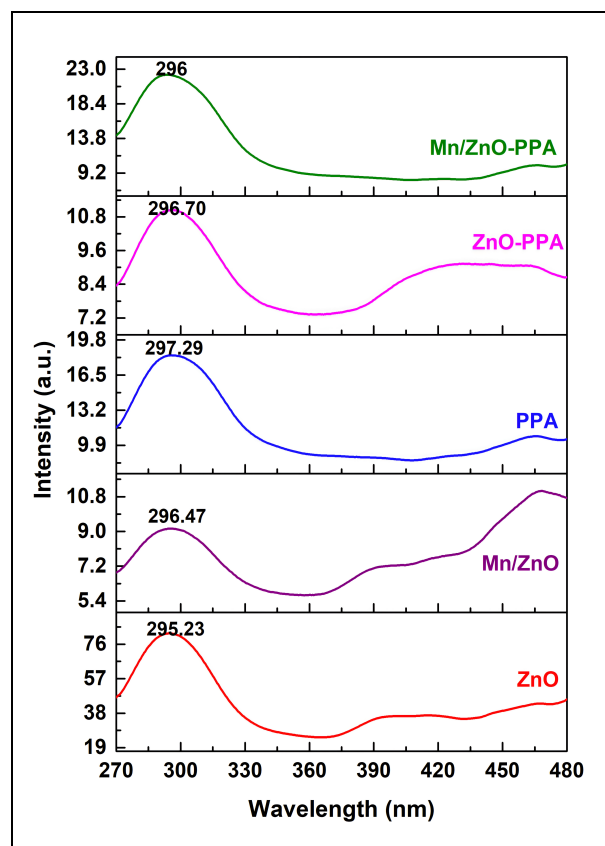


Fig. 6: Photoluminescence (PL) spectra of ZnO, Mn/ZnO, PPA, ZnO-PPA and Mn/ZnO-PPA

3.5 Photo Luminescence (PL) Spectra

Photoluminescence (PL) spectroscopy is a much-used technique to assess the optoelectronic properties of semiconducting materials. This technique is used to determine the direct HOMO-LUMO energy band gap of semiconducting materials. Fig. 6 shows the comparison between the emission spectra of pure ZnO, Mn/ZnO, PPA, ZnO-PPA and Mn/ZnO-PPA at the excitation wavelength of 295.23, 295.94, 297.29, 296.70, and 294.47, respectively. From the figure, the red shift at the peak 432, 401.64, 465, 462 and 465.05 nm for ZnO, Mn/ZnO and PPA, ZnO-PPA and Mn/ZnO-PPA was observed. The broad peak at 383.70 nm was observed for

ZnO-PPA nanocomposite (Samuel *et al.* 2019). The appearance of peak in poly-(p-anisidine) (PPA) polymer at the excitation wavelength of around 297 nm was observed, this PL emission typically involves transitions between the π^* (antibonding) and π (bonding) molecular orbitals and due to π - π^* transitions associated with its conjugated backbone.

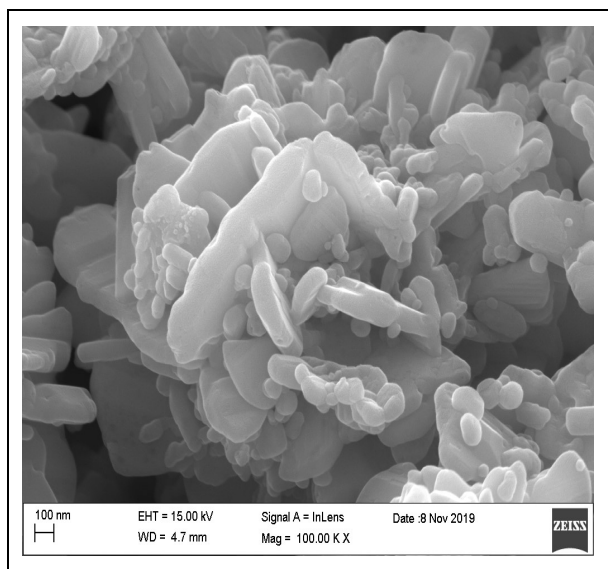


Fig. 7(a): SEM image of ZnO nanoparticle

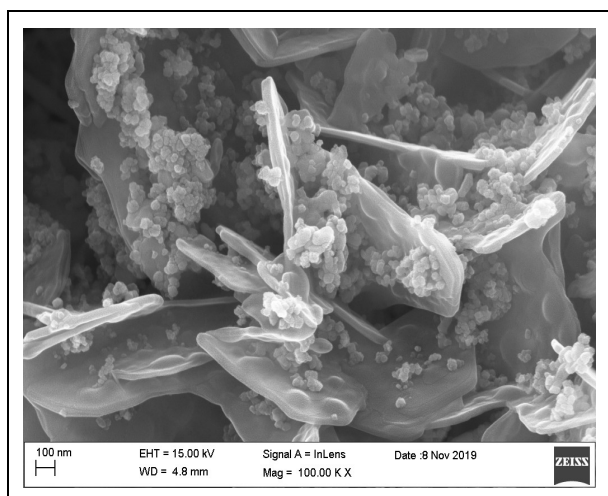


Fig. 7(b): SEM image of Mn/ZnO nanoparticle

3.6 Scanning Electron Microscopy (SEM) Analysis

The SEM analysis was used to study the morphology of pure ZnO, Mn/ZnO, PPA, ZnO-PPA and Mn/ZnO-PPA polymer nanocomposites. Here, the particles formed were in the region of at least 100 nm with good separation, thereby indicating and this preparation method was highly influenced by particle agglomeration (Wang *et al.* 2022). However, the SEM image of PPA through higher magnification revealed that

the products were agglomerated, and absolute separation had not occurred. For poly(p-anisidine), SEM images show a well-defined chain-like structure, indicative of polymer chain formation. When ZnO nanoparticles are embedded into PPA, the morphology shows ZnO dispersed within the polymeric network, with agglomeration mainly within the chains. Mn/ZnO-PPA composites exhibit closely clustered polymer chains and interconnected cross-linked structures with flower-like arrangements due to the embedded Mn/ZnO nanoparticles. These structural formations suggest effective embedding of nanoparticles within the PPA matrix, enhancing connectivity and reducing nanoparticle agglomeration.

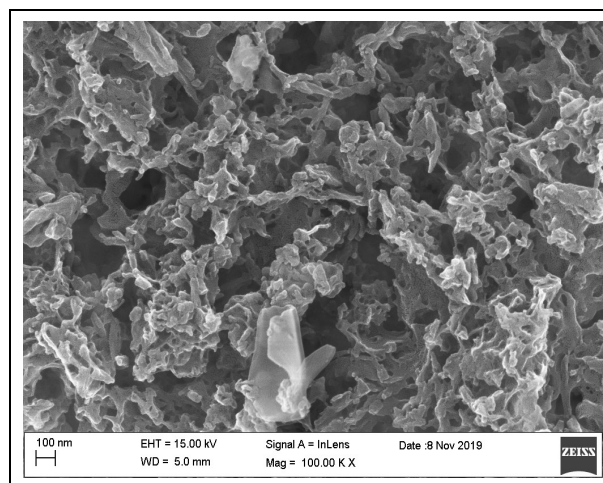


Fig. 7(c): SEM image of PPA polymer

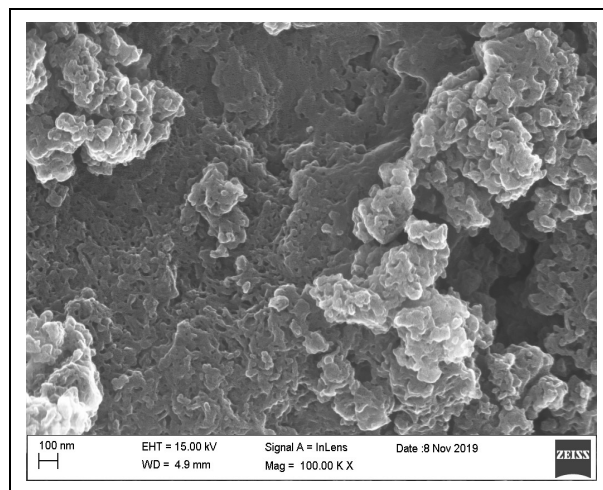


Fig. 7(d): SEM image of ZnO/PPA polymer nanocomposite

3.7 EDAX Analysis

The EDAX spectrum was used to measure the basic composition of the synthesized ZnO, Mn/ZnO, PPA, ZnO-PPA, and Mn/ZnO-PPA polymer nanocomposite and the results are represented in Fig. 8(a) to Fig. 8(e). Elements such as Zn, O and Mn, C and N

were present as expected in the respective compounds and no other impurities were present. The weight percentage is given table 1 (Faraz *et al.* 2018).

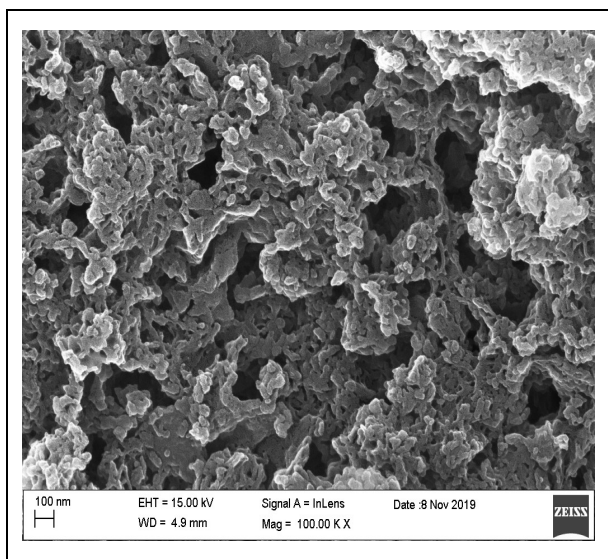


Fig. 7(e): SEM image of Mn/ZnO-PPA polymer nanocomposite

Table 1. Weight % of Zn, O, Mn, C and N

Samples	Zn Wt. %	O Wt. %	Mn Wt. %	C Wt. %	N Wt. %
ZnO	65.43	34.57	-	-	-
Mn/ZnO	78.41	15.17	6.41	-	-
PPA	-	22.97	-	65.69	11.34
ZnO-PPA	2.65	21.27	-	63.33	12.75
Mn/ZnO-PPA	2.24	22.03	0.01	63.32	12.40

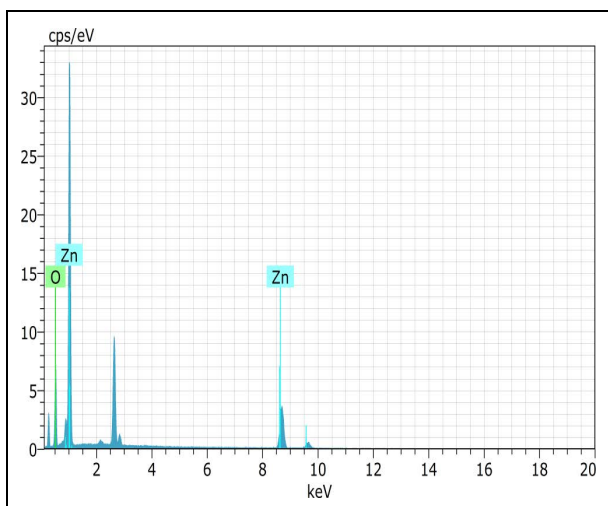


Fig. 8(a): EDAX spectra of Pure ZnO nanoparticle

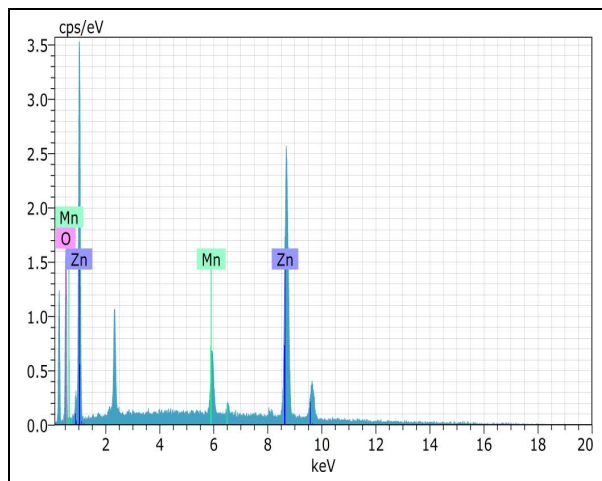


Fig. 8(b): EDAX spectra of Pure Mn/ZnO nanoparticle

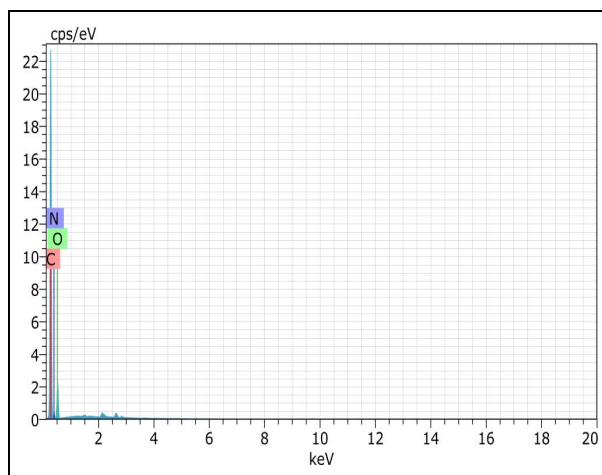


Fig. 8(c): EDAX spectra of PPA polymer

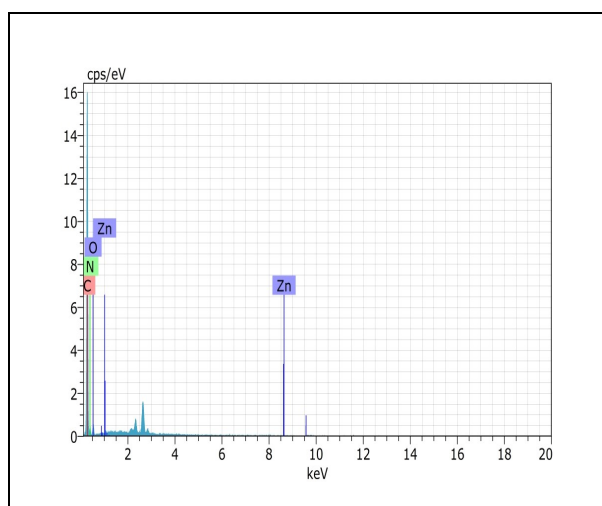


Fig. 8(d): EDAX spectra of ZnO/PPA polymer nanocomposite

3.8 Thermogravimetric Analysis (TGA)

All the synthesised materials underwent a three-stage thermal breakdown between 25°C and 900°C. Initially, the removal of free water molecules from the polymer matrix was thought to be the cause of a 5% weight loss at temperatures between 25 and 110 °C (K. K. Nagaraja et al. 2016). Secondly, it was shown that the removal of bound water and dopant ions from polymer chains was responsible for about 4-5% of the weight loss seen at temperatures between 110°C and 400°C. At stage three, the polymer began to degrade at 400 °C, and this was linked to the loss of dopant and the thermal breakdown of the polymeric chain skeleton. The last step of thermal decomposition was detected at 500 °C, and the complete breakdown of the substituent contained in the benzene ring of the polymeric backbone was responsible for the weight loss. The polymeric matrix is untied when a substituent cluster exists in the ortho position of the polymeric backbone, and steric effects are present. This requires a little amount of energy to break the polymer chain completely. The weight loss percentages for pure ZnO, Mn/ZnO, PPA, ZnO-PPA, and Mn/ZnO-PPA polymer nanocomposite were 3.02%, 11.43%, 63.76%, 66.33%, and 53.46%, respectively (G. Singh et al. 2020).

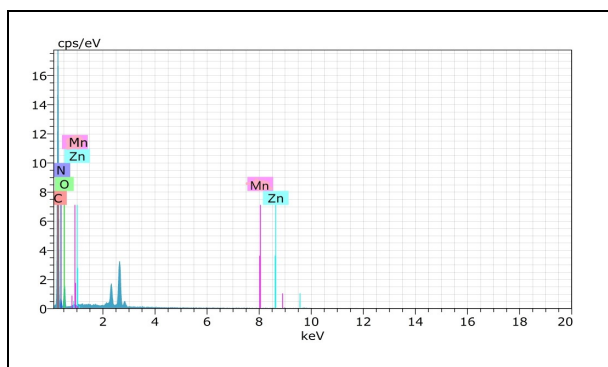


Fig. 8(e): EDAX spectra of Mn/ZnO-PPA polymer nanocomposite

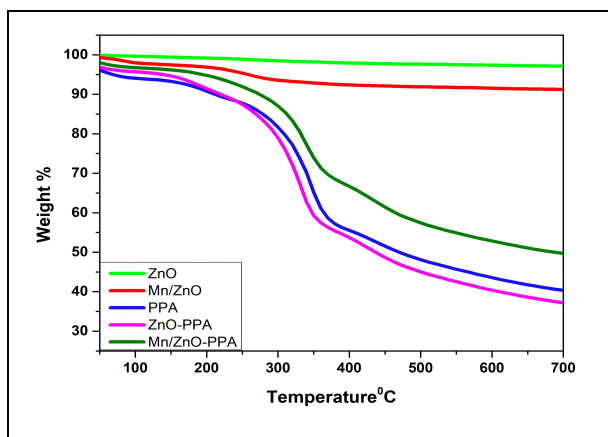


Fig. 9: TGA spectra of ZnO, Mn/ZnO, PPA, ZnO-PPA, and Mn/ZnO-PPA

4. CONCLUSION

In this investigation, pure ZnO, Mn/ZnO, PPA, ZnO-PPA, Mn/ZnO-PPA were synthesized. The morphological, optical, and thermal properties were analysed by various techniques. The calculated size was 57.04, 53.66, 61.84, and 50.85 nm for pure ZnO, Mn/ZnO, ZnO-PPA and Mn/ZnO-PPA, respectively. The SEM analysis confirmed the rod like structure with hexagonal crystallite shape and a spherical morphology for pure zinc oxide. The manganese doped nanoparticles and polymer nanocomposites have a nanoflower like shape. A very clear polymer cross-linkage chain formation for polymer nanocomposites was also observed. The UV-Visible spectral results showed a red shift in absorption with doping of manganese. The bandgap values are noted to be 3.20, 2.29, 2.89, 2.00 and 2.98 eV for pure ZnO, Mn/ZnO, PPA, and ZnO-PPA and Mn/ZnO-PPA nanocomposites, respectively. A three-stage thermal decomposition was observed in all the synthesised materials. The work can be extended with the manganese doped zinc oxide nanoparticles as an efficient photocatalyst for dye degradation applications.

FUNDING

There is no funding source.

CONFLICT OF INTEREST

The authors declared no conflict of interest in this manuscript regarding publication.

COPYRIGHT

This article is an open-access article distributed under the terms and conditions of the Creative Commons Attribution (CC BY) license (<http://creativecommons.org/licenses/by/4.0/>).



REFERENCES

- Ahmad, M., Ahmed, E., Ahmed, W., Elhissi, A., Hong, Z. L. and Khalid, N. R., Enhancing visible light responsive photocatalytic activity by decorating Mn-doped ZnO nanoparticles on graphene, *Ceram. Int.*, 40(7), 10085–10097(2014). <https://doi.org/10.1016/j.ceramint.2014.03.184>
- Begum, S. M., Ravindranadh, K., Ravikumar, R. and Rao, M. C., Spectroscopic studies on PVA capped ZnSe nanoparticles, *Optoelectron. Adv. Mater. Rapid Commun.*, 10(11–12), 889–892(2016).

- Bhargav, P. K., Murthy, K. S. R., Pandey, J. K., Mandal, P., Goyat, M. S., Bhatia, R. and Varanasi, A., Tuning the structural, morphological, optical, wetting properties and anti-fungal activity of ZnO nanoparticles by C doping, *Nano-Struct. Nano-Objects*, 19, 100365(2019). <https://doi.org/10.1016/j.nanoso.2019.100365>
- Bouzidi, A., Omri, K., Jilani, W., Guermazi, H. and Yahia, I. S., Effect of the different concentrations of ZnO: Mn incorporation on the microstructure and dielectric properties of epoxy nanocomposites, *J. Mater. Sci. Mater. Electron.*, 29(7), 5908–5917(2018). <https://doi.org/10.1007/s10854-018-8563-9>
- Djaja, N. F., Taufik, A. and Saleh, R., Manganese doping on the structural properties of TiO₂ and ZnO nanoparticles, *J. Phys. Conf. Ser.*, 1442, 012002(2020). <https://doi.org/10.1088/1742-6596/1442/1/012002>
- Faraz, M., Ansari, M. Z. and Khare, N., Synthesis of nanostructure manganese doped zinc oxide/polystyrene thin films with excellent stability, transparency and super-hydrophobicity, *Mater. Chem. Phys.*, 211, 137–143(2018). <https://doi.org/10.1016/j.matchemphys.2018.02.011>
- Sankar, G. R., Durgadevi, E., Navaneethan, M., Patil, V. L., Ponnusamy, S., Muthamizhchelvan, C., Kawasaki, S., Patil, P. S. and Hayakawa, Y., Low temperature ammonia gas sensor based on Mn-doped ZnO nanoparticle decorated microspheres, *J. Alloys Compd.*, 721, 182–190(2017). <https://doi.org/10.1016/j.jallcom.2017.05.040>
- Hoseinpour, V. and Ghaemi, N., Novel ZnO–MnO₂–Cu₂O triple nanocomposite: Facial synthesis, characterization, antibacterial activity and visible light photocatalytic performance for dyes degradation—A comparative study, *Mater. Res. Express*, 5(8), 085012(2018). <http://dx.doi.org/10.1088/2053-1591/aad2c6>
- Kanitta, Phongarhit, Pongsaton Amornpitoksuk, and Suwanboon, S., Synthesis, characterization, and photocatalytic properties of ZnO nanoparticles prepared by a precipitation-calcination method using a natural alkaline solution, *Mater. Res. Express*, 6(4), 04550(2019). <http://dx.doi.org/10.1088/2053-1591/aaf8db>
- Krishnaswamy, S., Ragupathi, V., Panigrahi, P. and Nagarajan, G. S., Photoluminescence quenching of green synthesized manganese doped zinc oxide by sodium iodide doped polypyrrole polymer, *Thin Solid Films*, 689, 137510(2019). <https://doi.org/10.1016/j.tsf.2019.137510>
- Leprince, W. Y., Jing, G. and El Zein, B., Novel ZnO-based nanostructures: Synthesis, characterization, and applications, *Cryst.*, 13(2), 338(2023). <https://doi.org/10.3390/cryst13020338>
- Nguyen, N. L. G., Pho, Q. H. and Nguyen, V. C., A high photo-catalytic activity of magnetic composite based on chitosan and manganese-doped zinc oxide nanoparticles for removal of dyeing wastewater, *J. Nanosci. Nanotechnol.*, 16(8), 7959–7967(2016). <http://dx.doi.org/10.1166/jnn.2016.12763>
- Qi, K., Xiaohan, X., Amir, Z., Mengyu, L., Qing, W., Shu-yuan, L., Huaxiang, L. and Guangzhao, W., Transition metal doped ZnO nanoparticles with enhanced photocatalytic and antibacterial performances: Experimental and DFT studies, *Ceram. Int.*, 46(2), 1494–1502(2020). <https://doi.org/10.1016/j.ceramint.2019.09.116>
- Rajamanickam, N., Mariammal, R. N., Rajashabala, S., and Ramachandran, K., Effect of (Li, Mn) co-doping on structural, optical and magnetic properties of chunk-shaped nano ZnO, *J. Alloys Compd.*, 614, 151–164(2014). <https://doi.org/10.1016/j.jallcom.2014.06.081>
- Safeen, A. and Safeen, K., The effect of Mn and Co dual-doping on the structural, optical, dielectric, and magnetic properties of ZnO nanostructures, *R. Soc. Chem. Adv.*, 12(12), 11923–11932(2022). <https://doi.org/10.1039/D2RA01798A>
- Samuel, E., Joshi, B., Kim, M. W., Kim, Y. I., Swihart, M. T. and Yoon, S. S., Hierarchical zeolitic imidazolate framework-derived manganese-doped zinc oxide decorated carbon nanofiber electrodes for high performance flexible supercapacitors, *Chem. Eng. J.*, 371, 657–665(2019). <https://doi.org/10.1016/j.cej.2019.04.065>
- Singh, G. and Chandra, S., Nano-flowered manganese doped ferrite@ PANI composite as energy storage electrode material for supercapacitors, *J. Electroanal. Chem.*, 874, 114491(2020). <https://doi.org/10.1016/j.jelechem.2020.114491>
- Wang, Y., Jing, C., Suye, Y., Enric, J. A., Muhammad, S., Ziyuan, W. and Wei, P., Synergistic effect of N-decorated and Mn²⁺ doped ZnO nanofibers with enhanced photocatalytic activity, *Sci. Rep.*, 6, 32711(2016). <https://doi.org/10.1038/srep32711>
- Xiao, D., Su, L., Teng, Y., Hao, J. and Bi, Y. Fluorescent nanomaterials combined with molecular imprinting polymer: Synthesis, analytical applications, and challenges, *Microchim. Acta*, 187(7), 1–15(2020). <https://doi.org/10.1007/s00604-020-04353-0>